# Mathematical modeling of radiation damage to microelectronic devices

V. S. Barashenkov, A. N. Sosnin, and S. Yu. Shmakov
*Joint Institute for Nuclear Research, Dubna*

N. G. Goleminov
*Moscow Engineering–Physics Institute*

A. Polanski
*Institute for Nuclear Problems, Swerk, Poland*

Fiz. Elem. Chastits At. Yadra **24**, 246–284 (January–February 1993)

The statistical Monte Carlo model of radiation damage to microelectronic devices of various configurations induced by protons, neutrons, and ions of various energies is discussed. Special attention is paid to high energies, where the primary bombarding particles generate developed showers of secondary particles. Devices made of silicon and gallium arsenide are considered as examples. The influence of the surrounding parts is studied. Depending on the energy deposited in the sensitive volume of a microelectronic cell, the model allows the calculation of the time dependence of radiation-induced breakdowns (upsets) of electronic devices. The modeling of radiative damage to microstrip detectors and bolometers with thin-film sensitive elements made of high-temperature superconducting material is discussed.

## INTRODUCTION

The trend toward microminiaturization of electronic devices makes it more and more important to ensure their stability to radiation such as cosmic rays and radiation from terrestrial sources. In devices containing semiconductor elements the danger of radiation-induced upsets arises primarily from the sharp drop in the capacitance of *pn* transitions to tens and even single femtofarads. This makes it possible for very large electrical pulses to appear during the collection of the charge generated by a particle crossing the sensitive volume of the detector. Although such phenomena are reversible and the device always returns to its initial state, the rather frequent radiation-induced upsets significantly decrease the device efficiency, especially under extraterrestrial conditions.

Many modern electronic devices contain elements in the form of a film "honeycomb" consisting of a large number of semiconductor (in future also superconductor) cells with size ranging from several micrometers to several tens of micrometers. In an external radiation field (protons, neutrons, and various types of ion beams), electromagnetic and nuclear processes develop in the cells, the backing, and the surrounding parts. This leads to the presence of additional charge and a significant amount of energy in the sensitive volumes of the microelectronic cells. If this charge and energy exceed a certain threshold (depending on the type of device and on the conditions under which it is used), radiation-induced upset can occur.

Satellite data show that in semiconductor devices with about $10^5$ cells, cosmic rays induce upsets about once every twenty-four hours.[1] During long flights (space stations should last several decades) this can prove to be a significant instability factor, particularly in view of the trend toward further miniaturization and increase of the number of semiconductor cells.

The use of electronic devices involving films made of high-temperature superconductors presents similar problems. Of course, the use of electronic devices involving high-temperature superconducting films has not yet spread beyond scientific research, where such devices are used in elements for collecting physical data. From the viewpoint of modeling radiation damage, their structure does not differ from that of an integrated circuit. Special conditions arise in large, densely packed systems, where the breakdown of superconductivity owing to the release of a large amount of heat in a small volume can lead to a rapidly propagating thermal wave which destroys the superconducting phase throughout the device. This can be a source of serious trouble.

The problem of calculating the radiation damage to microelectronic devices also arises in accelerator experiments, where devices often operate in very intense radiation.

Finally, we should mention microstrip detectors, where the radiation-induced leakage current determines the quality of the device.[2]

Particles propagating through a medium release energy just as in electromagnetic processes (ionization inside the cells of the thin-film honeycomb), but the high ionizing power of the nuclear fragments and recoil nuclei thus produced induce upsets in the operation of one or even several cells with large probability. In such interactions an energy of the order of tens and more MeV can be deposited in a cell. The upset probability is increased significantly by nuclear interactions in the surrounding parts of the detector.

The number of radiation-induced upsets of a microelectronic circuit is equal to the number of its completely damaged (put out of operation or not yet restored to operation) cells per bombarding particle:

$$\frac{n(t)}{N_0(t)}=\int_{E>0}\varphi(E)P(E)[1-R(E,t)]dE, \qquad (1)$$

where $t$ is the bombardment time, $N_0$ is the flux of primary nuclear-active particles, $\varphi(E)$ is the microunit breakdown

 1063-7796/93/010107-18$10.00  

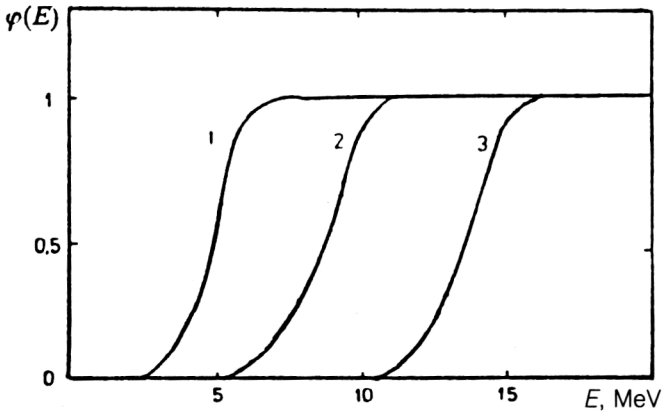


FIG. 1. Probability of upsets in a memory element of size 64 K (1), 16 K (2), and 4 K (3) when an energy $E$ is deposited in one of its cells.

probability for energy deposition in one cell, $P(E)$ is the probability for such energy deposition inside a cell (the "radiation spectrum" of a single event), and $R(E,t)$ is the restoration probability (the "healing"), which depends on the intensity of the radiation field and on the features of the electronic device.

The device functions $\varphi(E)$ and $R(E,t)$ depend on the specific parameters of the electronic device, and their determination is an independent problem. At present it is most convenient to find them experimentally.[3] In Fig. 1 we show examples of the function $\varphi(E)$ measured by methods described in Refs. 4 and 5 for several standard elements of an internal memory device in the energy range 0–20 MeV. The measurements were carried out in beams of electrons and heavy ions at the JINR Laboratory of Nuclear Reactions.[6] Here the condition $R=0$ was satisfied, and the number of radiation-induced upsets observed experimentally exactly corresponded to the function $\varphi$.

We see from Fig. 1 that for different memory elements the measured functions $\varphi(E)$ are quite similar and differ only by a shift along the $E$ axis. The upset probability, especially in devices with a large number of cells, can be approximated as a step function:

$$\varphi(E)=\begin{cases}0, & E<E^* \\ 1, & E>E^*.\end{cases}$$

A similar form of the function $\varphi(E)$ also holds for particles with higher energies.

The radiation spectrum of a single event $P(E)$, which depends on the type of bombarding particle, the chemical composition, and the device configuration, can be calculated theoretically fairly accurately using the Monte Carlo method with the internuclear-cascade model, which takes into account the contribution of showers induced by hadrons traveling through the material and strongly ionizing nuclear fragments and recoil nuclei.

The primary reason for radiation-induced upsets is energy deposition by particles in the sensitive volume of the device. Therefore, studies of the energy-loss spectra of various particles with a wide range of charge and mass are essential for analyzing this class of phenomena. The application of the results to specific types of electronic systems is an independent problem lying outside the scope of this review.

## THE INTERNUCLEAR-CASCADE MODEL

The propagation of a beam of high-energy particles in a medium is such a complicated phenomenon that it is extremely difficult to describe it analytically by equations, especially in view of the complicated geometry of the problem and the multicomponent nature of the medium material. Difficulties arise already at the stage of specifying the various initial data for describing the features of nuclear reactions. The best approach to a theoretical analysis is therefore statistical modeling using the Monte Carlo method. Here it becomes possible not only to include the diverse details about the nuclear interactions, but also to model the specific features of actual setups and experiments.

A method for the statistical modeling of the various processes arising in the propagation of high-energy particles and nuclei in condensed and gaseous media has been developed over the last few years at JINR.[7,8] By using canned programs it is possible to analyze interactions of hadrons and light nuclei with heterogeneous matter of practically any geometry and content for energies from a fraction of an eV (induced thermal neutron beams) to several tens of GeV. The use of models of quark–gluon strings—short-lived physical objects formed in interactions of fast hadrons—makes it possible to extend the calculations to even higher energies. The methods developed can be used to calculate the intensity and spectra of various types of particle inside the bombarded matter and the spatial distribution and parameters of the nuclear-reaction products, which, as noted above, are particularly effective in inducing radiation defects.

The interaction of a high-energy particle with matter is a cascade type of process which develops rapidly in time: a "cascade tree" with a large number of branches and nuclear interactions at the junctions. The calculation of the cascade tree requires the modeling of three fundamental processes:

- The particle interaction with a nucleus encountered along its path; in the case of an inelastic interaction this is accompanied by secondary particle production and sometimes by nuclear disintegration or fission.
- The particle mean free path in the medium from one nuclear interaction to another, taking into account the energy loss of a charged particle to electromagnetic processes in the medium.
- The possible decay of an unstable particle between two nuclear interactions. This, as a rule, happens with $\pi^0$ mesons, and in extended media also with $\pi^{\pm}$ mesons. As the particle energy increases the decay probability decreases according to relativistic laws.

It is easy to see that the calculation is cyclical in nature and reduces to several repetitions of a few basic operations (Fig. 2). After one cascade tree is calculated, the calculations are repeated for a new primary particle, then for another, and so on. This approach corresponds to actual

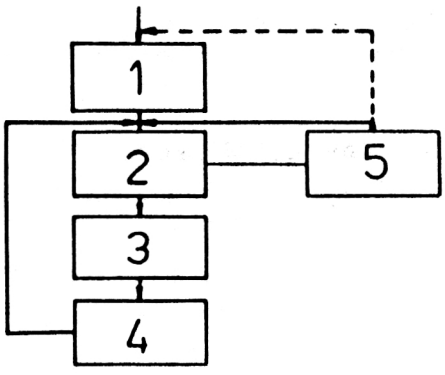


FIG. 2. Basic scheme for calculating an internuclear cascade in matter. *1*) Random selection of the energy and other parameters of the primary particle; *2*) check whether or not the particle is a $\pi$ meson; if yes, calculate its decay probability; *3*) the particle did not decay; compute its mean free path; *4*) calculate the nuclear interaction. Determine the characteristics of the particles produced and the residual nucleus (or its fission fragments); *5*) the particle decayed, choose a new particle. If a primary particle was considered, go to block 1 (dashed line). The actual computational scheme includes many additional details and is therefore considerably more complicated.

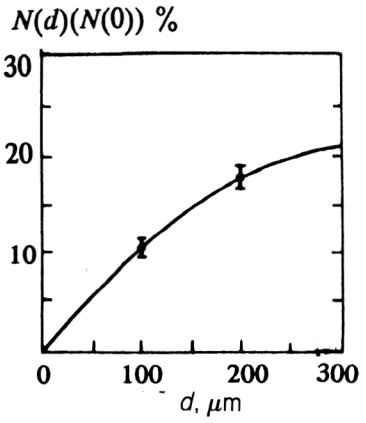


FIG. 3. Increase of the number of damaged cells of a silicon microcircuit due to particles emitted from the backing of thickness $d$. The primary particles are 3.65-GeV protons. The points show the statistical accuracy of the Monte Carlo calculation. It was assumed that the cell is knocked out of operation if an energy greater than 2 MeV is deposited in it.

physical processes occurring in nature, where the end effect results from the independent contributions of a large number of cascades.

The only special feature of calculations for film integrated circuits is the fact that in the direct modeling of cascades, most of the particles bombarding the film pass through it without undergoing a single nuclear interaction. Here we are actually calculating the macroscopic cross section for a particle to interact with the film, because ensuring that a sufficient number of interactions occur in it requires too much computer time. The calculation becomes simpler if the cross section for the particle to interact with the film is specified *a priori* on the basis of experimental data about the nuclear-reaction cross sections, and if it is used later as a statistical weight in the Monte Carlo simulation. In other words, it can be assumed that each primary particle interacts with the film, and the resulting data then pertain to an effective flux

$$N=N_0[1-\exp(-d\Sigma_{\text{tot}})], \tag{2}$$

where $N_0$ is the actual flux of bombarding particles, $d$ is the film thickness, and $\Sigma_{\text{tot}}$ is the macroscopic cross section for elastic and inelastic nuclear interactions.

Actually, the situation is somewhat more complicated, since the crystalline honeycomb of semiconductor cells is attached to a backing in which ionizing-particle cascades also develop. Here several particles move at large angles to the primary-beam direction ($\theta > 90°$) and also can lead to radiation-induced damage of the semiconductor cells. Of course, at high energies the contribution of these particles is small. For example, calculation shows that in the bombardment of 100 $\mu$m of film by protons with energies of several GeV, the inclusion of the silicon backing of thickness $d=200$ $\mu$m increases the number of damaged cells by 20% (Fig. 3). However, as the energy decreases the radiation effect of the backing becomes more important.

To preserve the high efficiency of the Monte Carlo simulation and include the contribution of the backing, it is convenient here again to use statistical weights: for example, to randomly select the nuclear-interaction depth using an exponentially decreasing weight function with appropriately selected exponent, which is mainly determined by the radiation mean free path of the $\alpha$ particles or recoil nuclei produced in the backing at low energies. The other nuclear components give a smaller contribution (see below). The coefficient depends weakly on the energy of the bombarding beam.[1)]

## CALCULATION OF THE MEAN FREE PATHS

The particle mean free path in the medium between two successive nuclear interactions is determined from the equation

$$\int_0^l dl/\lambda(E(\mathbf{r}),\mathbf{r}) = -\ln\xi, \tag{3}$$

where $\lambda = 1/\Sigma_i \sigma_i(E(\mathbf{r}))\rho_i(\mathbf{r})$ is the mean free path at the point $\mathbf{r}$, $\sigma_i$ is the total cross section for the interaction of a particle with a nucleus of type $i$ at the point $\mathbf{r}$, $\rho_i$ is the number density of these nuclei, and $\xi$ is a random, uniformly distributed number. The integration runs along the particle trajectory. This equation is a generalization of the familiar relation $l=-\ln\xi$ with constant $\lambda$ to inhomogeneous media and takes into account the variation of the particle energy $\varepsilon=E(\mathbf{r})$ along the trajectory as a result of electromagnetic processes.

The hadron–nucleus interaction cross sections $\sigma_i$ for the nuclei most frequently encountered in practice are given in tables in Ref. 9, and for intermediate nuclei they can be accurately calculated by using approximating expressions.[10,11] At low energies ($E<14.5$ MeV) the standard group constants from Ref. 12 can be used.

The cross sections for the interaction of two nuclei are more complicated. There are few experimental data on them, and it is necessary to use the approximation

$$\sigma=\pi r_0^2[A_H^{1/3}+A_M^{1/3}+bA_H^{1/3}A_M^{1/3}/(A_H^{1/3}+A_M^{1/3})+d(1 -Z_H/A_H-Z_M/A_M)-C(E)]^2(1-V/E_c), \quad (4)$$

where $A_H$ and $A_M$ are the mass numbers of the incident nucleus and the target nucleus, $Z_H$ and $Z_M$ are the corresponding charge numbers, $V$ is the Coulomb barrier for a given pair of nuclei, $E_c$ is the energy of their relative motion, $r_0$, $a$, $b$, and $d$ are numerical parameters, and $C(E)$ is a function (different for $\sigma_{el}$ and $\sigma_{in}$) weakly dependent on the energy, selected from comparison with experiment separately for deuterons, $\alpha$ particles, and groups of heavier nuclei.

At low energies we use the approximate expression

$$\sigma_{in}=\pi r_c^2(A_H^{1/3}+A_M^{1/3})^2(G/E_c) \times\ln\{1+\exp((E_c-V)/g)\}, \quad (5)$$

where $r_c=(1.4-1.6)\times10^{-13}$ cm and $g$ is a phenomenological parameter. The coefficient $G$ is determined from the condition that (4) and (5) match smoothly for $E\cong10$ MeV/nucleon.

It should be noted that uncertainties in the choice of the cross sections strongly affect the results of the calculation. This is one of the most important features of the calculations.

Regarding the calculation of the energy lost by singly charged $p$, $d$, and $t$ particles and multiply charged ions in electromagnetic processes, at low energies these are calculated using the Lindhard method.[13] We should stress that for microelectronic circuits this region is particularly important, since the mean free paths of the most strongly ionizing low-energy particles are comparable to the dimensions of individual cells, and errors in the specific losses $dE/dx$ very strongly affect the results of the calculation. In addition, it should be borne in mind that tracks of low-energy particles differ significantly from straight lines. The inclusion of these deviations is quite difficult. In our model all tracks are assumed to be straight lines. This limits the applicability of the model to cell dimensions larger than several micrometers.

At high energies we use the Bethe–Bloch approximation with corrections for density effects and the effect of electron coupling in inner atomic shells.[14–16] In the intermediate region we use the analytic approximation

$$dE/dx=(C_1\sqrt{E}+C_2+C_2/\sqrt{E})^{-1}, \quad (6)$$

where the coefficients $C_i$ are determined by comparison with the Lindhard expressions at low energies and the Bethe–Bloch expression at high energies.[17,18]

At very high energies our model includes the effect of the electromagnetic form factors and the electron–positron pair contribution.[19–21]

The calculated value of $dE/dx$ is in good agreement with the tabulated values[22,23] obtained by analysis of the corresponding experimental data.

Equation (3) is solved by the technique of equalizing the cross sections.[24] Here the values of $dE/dx$ for protons, mesons, and the bombarding nucleus (or nuclei, if the primary beam consists of a mixture of them) are calculated at the first stage of the calculations and then interpolated; for the nuclear fragments and recoil nuclei produced in the internuclear cascade the losses $dE/dx$ are calculated anew each time.

To speed up the calculation of the mean free path $R=\int dE/(dE/dx)$ of mesons and nuclei at energies above several MeV, it is convenient to perform the calculations using the scaling relation

$$R(E/A)=R(E^*/A)+(A/Z^2)[R_p(E/A) -R_p(E^*/A)], \quad (7)$$

where $R_p$ is the proton mean free path, $E^*$ is a minimum energy above which the scaling relation is applicable, and $A$ and $Z$ are the nuclear mass and charge numbers (for $\pi$ mesons $A=0.15$).

## MODELING OF NUCLEAR INTERACTIONS

The calculation of the junctions of the cascade tree is the most complicated and awkward part of the problem. In principle, these junctions can be described using phenomenological approximations of known experimental data. In this manner it is almost always possible to obtain a good description of elastic collisions, where only the momenta of the colliding nuclei and particles change and all their other properties stay the same. As far as inelastic collisions are concerned, their properties depend significantly on the particle energy and the type of target nucleus, so phenomenological approximations turn out to be effective only in certain special cases, for example, when the averaged characteristics of the radiation and targets of simple chemical composition are of interest. However, also in these cases the development of phenomenological approximations for a wide energy range is itself a very difficult problem, and is warranted only in the case of multiple repetitions of the calculations for matter of a given composition.

Since we wanted to consider a variety of situations, we rejected this approach and instead performed a new calculation of the inelastic nuclear interaction each time. The exception was the energy range below 10.5 MeV, where all the calculations of the internuclear cascade are carried out using the well known 26-group set of constants of Abagyan *et al.*[12]

In our work we use the cascade–evaporation model of nuclear reactions.[25–28] In accordance with experiment, it is assumed that inelastic interactions of particles with energies below a few tens of MeV are accompanied by the formation of a so-called "compound nucleus"—a strongly excited system decaying with emission of one or two neutrons or $\gamma$ quanta. At energies above several tens of MeV it is assumed that inelastic interactions occur in three successive stages. The process begins with the rapidly developing "cascade stage," when the newly created particles and knocked-out intranuclear nucleons leave the nucleus, with the nucleus remaining in a highly excited state. During the

TABLE I. Number of nuclei with charge $Z$ produced in the inelastic interaction of a proton and a $^{12}C$ ion with a silicon nucleus at 3.65 GeV/nucleon (Ref. 6).

| $Z$ | $p$ + Si | | | $^{12}C$ + Si | | |
|---|---|---|---|---|---|---|
| | *A* | *B* | *C* | *A* | *B* | *C* |
| 1 | 0,50 | 0,27 | — | 0,50 | 0,34 | — |
| 2 | 0,71 | 0,55 | 0,30 | 0,59 | 0,44 | 0,27 |
| 3 | 0,004 | 0,006 | 0,01 | 0,03 | 0,003 | 0,01 |
| 4 | 0,04 | 0,02 | 0,04 | 0,06 | 0,02 | 0,03 |
| 5 | 0,03 | 0,01 | 0,03 | 0,03 | 0,02 | 0,02 |
| 6 | 0,09 | 0,06 | 0,09 | 0,10 | 0,04 | 0,07 |
| 7 | 0,03 | 0,02 | 0,04 | 0,04 | 0,03 | 0,02 |
| 8 | 0,08 | 0,08 | 0,10 | 0,05 | 0,04 | 0,06 |
| 9 | 0,04 | 0,04 | 0,05 | 0,03 | 0,02 | 0,03 |
| 10 | 0,08 | 0,08 | 0,09 | 0,04 | 0,04 | 0,06 |
| 11 | 0,06 | 0,07 | 0,08 | 0,04 | 0,05 | 0,04 |
| 12 | 0,13 | 0,11 | 0,18 | 0,08 | 0,07 | 0,09 |
| 13 | 0,13 | 0,18 | 0,08 | 0,07 | 0,11 | 0,04 |
| 14 | 0,09 | 0,14 | 0,04 | 0,07 | 0,10 | 0,02 |

Note. *A* is the calculation based on the cascade-evaporation model (2000 primary proton interactions and 1500 $^{12}C$ ion interactions were studied). *B* is the calculation including nonequilibrium precompound decay processes (1000 primary proton interactions and 1000 $^{12}C$ ion interactions). *C* is the calculation using the percolation model (2500 proton interactions and 2500 $^{12}C$ ion interactions).

second stage this nucleus relaxes to the equilibrium state (here again individual fast particles can be emitted, which carry off a large fraction of the excitation energy). The interaction concludes with the relatively slowly developing "decay stage," during which the nucleus loses its excitation energy by the competing processes of particle evaporation and nuclear fission (the fission fragments produced, as a rule, are also highly excited and lose their energy by particle evaporation). The decay stage concludes with the emission of $\gamma$ quanta, after which the nucleus is in a long-lived state.

During the development of the intranuclear cascade, some of the nucleons of the target nucleus (and, in the case of nucleus–nucleus collisions, some of the nucleons of the incident nucleus) are knocked out even before the cascade stage is completed, so that the intranuclear densities at the beginning and end of the process are different, which significantly affects the results of the calculation. In order to take into account this factor (the trailing effect), the modeling of each hadron–nucleus event or nucleus–nucleus interaction begins with the random selection of the spatial coordinates of all the intranuclear nucleons. The intranuclear density distributions measured in electron scattering experiments are used for this. At the initial instant of time $t$ corresponding to the touching of the colliding nuclei (or of the bombarding hadron and the target nucleus), all the intranuclear collisions allowed by the kinematics and the Pauli principle are randomly selected. The one which occurs earliest, i.e., at the time $t'=t+\min(t_i)$, is selected, after which the positions of the colliding nuclei and all the cascade particles (nucleons and created $\pi$ mesons) are shifted to the new position corresponding to the time $t'$. Then the procedure is repeated until all the cascade particles are exhausted, after which the calculation of the post-cascade interaction stage begins.

It should be noted that this part of the model is the least developed. In particular, the selection of the phenomenological parameters to be used is made difficult by the lack of reliable experimental data on the nuclear excitation energy and momenta (some of the data are contradictory[29]). In the calculations carried out thus far using the internuclear-cascade model, namely, those for electronuclear reactors,[45] isotope yields of practical importance,[43,44] averaged data for radiation shielding, and other problems, the uncertainties in the properties of the produced excited nuclei weakly affected the results, so relatively little attention has been paid to them. The intranuclear-cascade model has not been developed in recent years for energies below several GeV/nucleon. The fact that the radiation energy deposit is almost completely due to the nuclear component of the cascade requires more careful study of hadron–nucleus and ion–nucleus interactions.

Some idea of the accuracy of the calculations of the post-cascade stage of nuclear reactions can be obtained by comparing the various approaches: the evaporation model, the inclusion of preequilibrium emission of particles and fragments, and the percolation model. At moderate excitation energies apparently the most accurate is the evaporation model (including the competition of high-energy fission), supplemented by the inclusion of nonequilibrium pre-compound particle-emission processes. Although the number of nonequilibrium fragments is relatively small, as a rule their energy is greater than that of the evaporation

particles, and on the average they produce a greater energy deposit in the cells. Neglect of these decay channels of post-cascade nuclei introduces very important errors.

A serious defect of this approach is the fact that it does not describe the production of heavy fragments—fragments heavier than $\alpha$ particles. So far there is no satisfactory theory of fragmentation processes; the only hope is that, owing to the experimentally established fact that the cross sections for such channels are small, nonequilibrium fragmentation gives a comparatively unimportant contribution to radiation damage.

An alternative method for a probabilistic calculation of decays of excited nuclei is the percolation approach.[30–32] We see from Table I that the results obtained here sometimes differ by a factor of one and a half to two from those calculated by other methods. However, few calculations based on the percolation approach have been carried out so far, and it is difficult to say how much better it is than the others.

Comparison with experiment shows that for hadron–nucleus interactions the cascade–evaporation model is applicable up to energies $E=5$ GeV. In the case of a collision of two nuclei, its range of applicability is smaller, $E=2$–3 GeV/nucleon of the incident light nucleus, and for collisions of heavy nuclei it is even smaller.[28] At high energies the multiplicity of created low-energy particles characterizing the degree of branching (the "strength") of the theoretical cascade exceeds the experimental value and grows rather rapidly with increasing energy. This is not very important for the calculation of cascades in thick pieces of matter, since the main contribution in that case comes from interactions with lower energies, which are described well by the cascade–evaporation model. The situation in the case of thin layers and films is different, because there are practically no secondary nuclear collisions and the errors in the characteristics of the high-energy interaction become quite noticeable.

The disagreement with experiment can be eliminated if the hadron–hadron interaction mechanism is improved by including the contribution of quark–gluon strings. Unfortunately, this considerably complicates the computational algorithm and leads to the expenditure of a large amount of computer time. In addition, string models are not yet very well defined. Nevertheless, if we restrict ourselves to energies below a few tens of GeV/nucleon (the energies important for cosmic rays), we can use approximate semiphenomenological quark–gluon string models (see, for example, Refs. 33 and 34), which, in spite of some theoretical objections, give a good description of experiment, as can be seen from Tables II and III (see Ref. 35 for more detail).

In practical calculations of internuclear cascades the contribution of quark–gluon effects can be neglected for $E<3$–4 GeV/nucleon, but at higher energies the differences grow rapidly. For example, the average numbers of nuclear interactions (junctions of the cascade tree) in copper or iron targets calculated using the ordinary cascade–evaporation model and including quark–gluon strings differ by about 20% at $E=3.5$ GeV/nucleon, and already by 50% at $E=9$ GeV/nucleon (the primary particles are protons and $^{12}$C ions).

TABLE II. Average values of the momentum, emission angle, and multiplicity of $\pi$ mesons at $E=3.3$ GeV/nucleon. SM and CM are the results of the calculations using the string and cascade models. The experimental data are taken from Refs. 36 and 37.

| Reaction | Model | $\langle p\rangle$, GeV/$c$ | $\langle\theta\rangle$, deg | $\langle n\rangle$ |
|---|---|---|---|---|
| $p$+C | SM | 0.49±0.001 | 47.3±0.1 | 0.24±0.001 |
| | CM | 0.43±0.02 | 55.0±2.0 | 0.48±0.02 |
| | exp. | 0.53±0.03 | 49.4±1.7 | 0.33±0.02 |
| $d$+C | SM | 0.60±0.001 | 45.3±0.1 | 0.50±0.001 |
| | CM | 0.53±0.01 | 47.5±1.0 | 0.78±0.02 |
| | exp. | 0.58±0.03 | 44.2±1.0 | 0.60±0.03 |
| $a$+C | SM | 0.61±0.02 | 41.6±1.2 | 0.72±0.03 |
| | CM | 0.56±0.01 | 46.1±1.1 | 1.16±0.03 |
| | exp. | 0.63±0.03 | 43.2±1.1 | 1.02±0.03 |
| C+C | SM | 0.62±0.01 | 40.0±0.9 | 1.23±0.03 |
| | CM | 0.59±0.01 | 41.4±1.0 | 1.70±0.04 |
| | exp. | 0.62±0.03 | 40.0±0.7 | 1.50±0.05 |
| C+Ta | SM | 0.49±0.01 | 54.0±1.5 | 3.4±0.1 |
| | CM | 0.36±0.02 | 66.0±4.5 | 5.9±0.4 |
| | exp. | 0.48±0.01 | 51.6±0.6 | 3.2±0.1 |

As noted above, the main contribution to radiation-induced damage to microelectronic circuits comes from nuclear fragments and residual recoil nuclei. Let us study the accuracy of calculating them for the example of the interaction of carbon ions with silver nuclei at $E=85$ GeV/nucleon, where experimental data are available.[39]

The cross sections for producing light fragments with mass close to that of the $^{12}$C ion together with their angular and energy distributions are shown in Figs. 4–6. In Figs. 7 and 8 we give the data for heavy recoil nuclei—fragments of the target nucleus.[40] We see that the agreement is quite good. Marked differences are observed for $^{6}$Li, but this fragment plays a small role in radiation damage (see below), and if desired the discrepancies are easily eliminated by appropriate selection of the model parameters.

The discrepancies between the calculated and experimental spectra for $^{52}$Mn in Fig. 8 in the region $E\leqslant 10$ MeV

TABLE III. Average characteristics of cascade protons at $E=3.3$ GeV/nucleon ("evaporation" particles are not included). The notation is the same as in Table I. The experimental data are taken from Ref. 38.

| Reaction | Model | $\langle p\rangle$, GeV/$c$ | $\langle\theta\rangle$, deg | $\langle n\rangle$ |
|---|---|---|---|---|
| $p$+C | SM | 1.47±0.003 | 38.7±0.08 | 1.76±0.004 |
| | CM | 1.16±0.04 | 43.3±1.5 | 2.15±0.08 |
| | exp. | 1.44±0.06 | 38.2±1.0 | 1.83±0.1 |
| $d$+C | SM | 1.53±0.003 | 39.4±0.08 | 1.88±0.004 |
| | CM | 1.12±0.02 | 42.6±0.9 | 2.46±0.05 |
| | exp. | 1.50±0.04 | 38.0±0.07 | 1.95±0.08 |
| $a$+C | SM | 1.77±0.05 | 34.1±1.0 | 2.63±0.08 |
| | CM | 1.48±0.04 | 35.4±0.9 | 3.33±0.09 |
| | exp. | 1.63±0.04 | 34.7±0.5 | 3.06±0.10 |
| C+C | SM | 2.00±0.04 | 29.1±0.6 | 4.06±0.09 |
| | CM | 1.93±0.05 | 28.0±0.7 | 4.99±0.10 |
| | exp. | 2.00±0.03 | 28.4±0.4 | 4.30±0.10 |
| C+Ta | SM | 1.13±0.03 | 48.4±1.4 | 14.0±0.4 |
| | CM | 0.96±0.06 | 47.0±3.1 | 17.0±1.1 |
| | exp. | 1.05±0.01 | 49.6±0.4 | 15.2±0.6 |

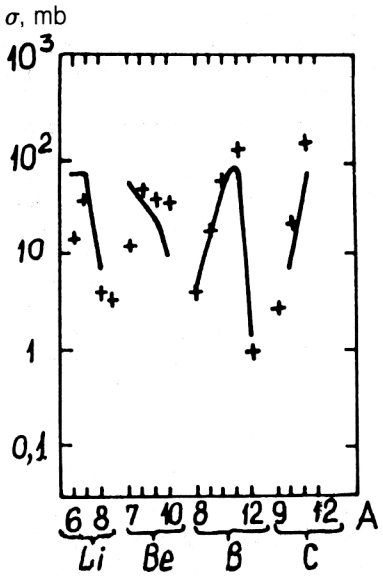


FIG. 4. Cross sections for light-fragment production in the reaction $^{12}C+^{109}Ag$. The curves are from the experiment of Ref. 39, and + are the calculated values.

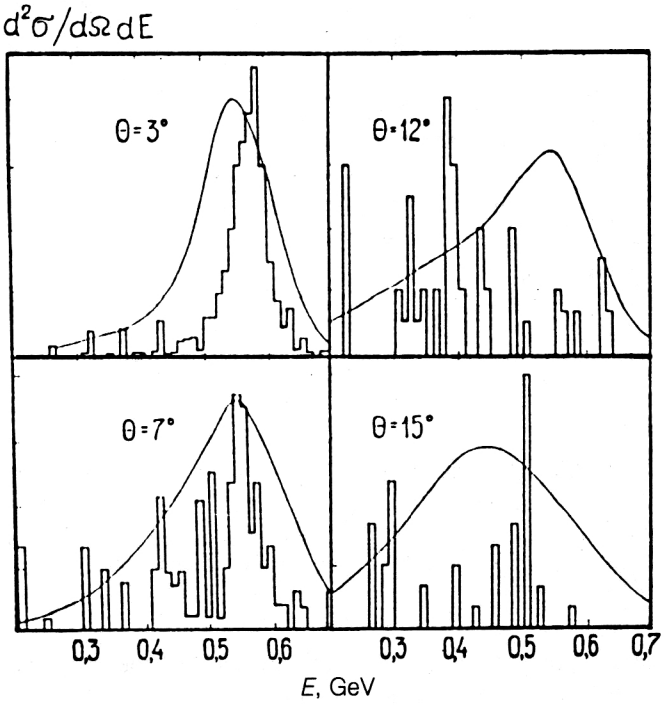


FIG. 6. Energy spectra of $^{9}Be$ fragments in the reaction $^{12}C+^{109}Ag$ for various emission angles $\theta$. The curves are the fit to the experimental data of Ref. 39, and the histograms are calculated ($\theta=2.5°$).

are apparently related to certain experimental errors. (It is difficult to understand why so many nearly stopped nuclei are observed; see Ref. 40 for more detail.) The average values $\langle E\rangle^{\text{theor}}=12$ and 29.3 MeV for $^{52}Mn$ and $^{89}Zr$ nuclei are close to the corresponding experimental values $\langle E\rangle^{\text{exp}}=9.9$ and 31.5 MeV.

In Figs. 9 and 10 the characteristics of fragments and recoil nuclei calculated using our intranuclear-cascade model are compared with the values calculated by other authors. The agreement is quite satisfactory. A significant difference is observed only for $\alpha$ particles. This is apparently related to the additional inclusion of nonequilibrium processes in our model. (Data for $d$, $t$, and $^{3}He$ are not given in Ref. 40.)

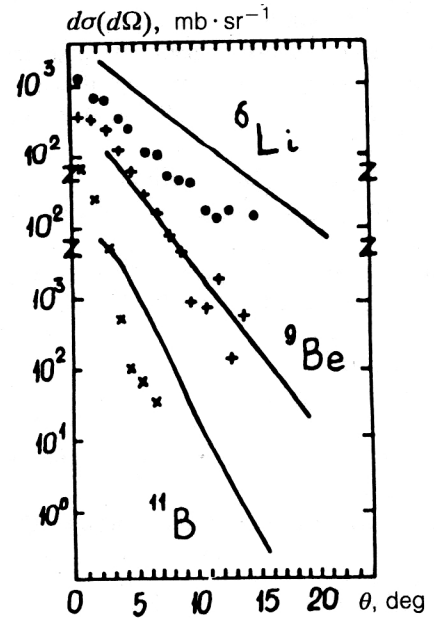


FIG. 5. Angular distributions of light fragments in the reaction $^{12}C+^{109}Ag$. The curves are from the experiment of Ref. 39, and ●, ×, and + are the corresponding calculated values.

In Fig. 11 we compare the mass-number distributions of nuclear fragments and residual nuclei produced in interactions of protons and carbon ions with Si and GaAs nuclei. In Figs. 12 and 13 we show the energy spectra of $\alpha$ particles and all the other residual nuclei with charge numbers $Z>2$ at incident-particle energies of 0.1 and 1 GeV/nucleon. In interactions of the proton beam with the target, the growth of the incident-particle energy is accompanied by increased multiplicity and average energy of the helium nuclei produced. This effect is seen especially clearly for the GaAs target. Compared with a silicon target, the spectra of $\alpha$ particles produced in $p$+GaAs collisions is considerably harder. This is related to the larger Coulomb barrier, which hinders the formation of slow $\alpha$ particles. The situation is reversed for heavy recoil nuclei: owing to the smaller mass of silicon, its fragments are on the average formed with higher energy.

When the incident proton is replaced by a carbon nucleus, a sizable high-energy tail appears in the heavy-fragment spectrum. As the energy increases the shape of the fragment spectra changes slightly. For a GaAs target the use of carbon ions as the projectile leads to a significant increase of the absolute yield of slow $\alpha$ particles, which is particularly important in view of their large defect-formation capability (see the section "Modeling of radiation-induced damage to microstrip detectors" below). The increased yield of slow particles is explained by the

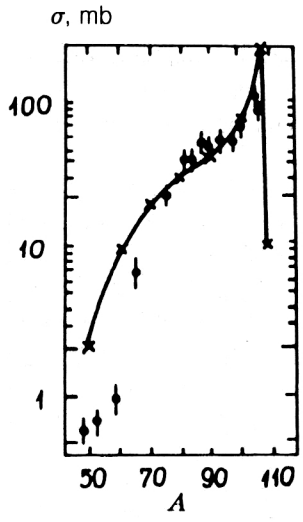


FIG. 7. Mass distribution of $^{109}$Ag fragments of the target nucleus. ● are from the experiment of Ref. 39, and × and the approximating curve are our calculation.

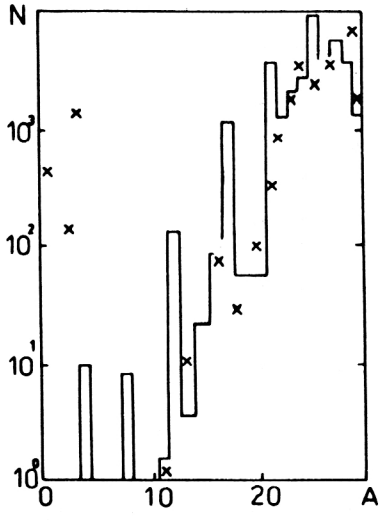


FIG. 9. Mass distribution of residual nuclei in the reaction $p+^{28}$Si at $E=100$ MeV. The histogram is the calculation of Ref. 40, and the × are our data.

larger degree to which the target nucleus is broken up and, consequently, the smaller Coulomb barrier.

It follows from these results that at low bombarding-particle energies the energy deposition and, consequently, the number of radiation upsets in silicon cells must be larger than in gallium arsenide. The difference becomes smaller with increasing energy, and at high energies the number of upsets of microcircuits prepared on a base of gallium arsenide becomes larger than for silicon cells. The authors of Ref. 41, who calculated the radiation damage to cells in proton beams of energy 25–300 MeV, arrived at a similar conclusion.

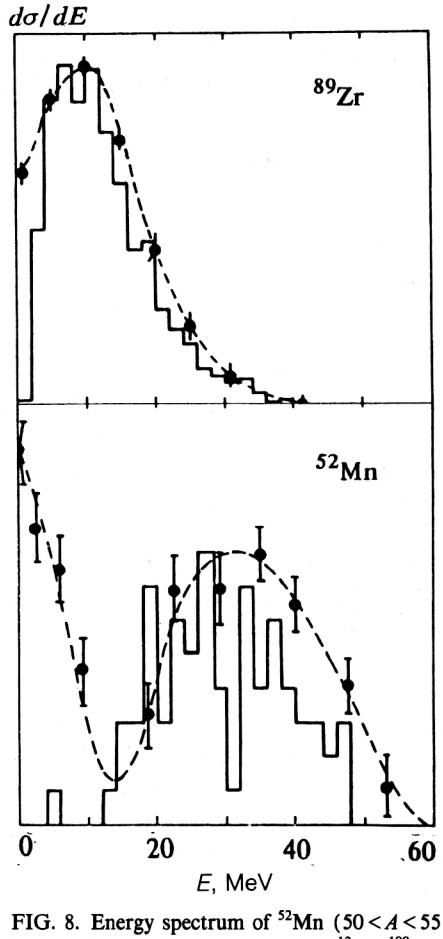


FIG. 8. Energy spectrum of $^{52}$Mn ($50<A<55$) and $^{89}$Zr ($85<A<89$) fragments produced in the reaction $^{12}C+^{109}$Ag. The dashed line is from the experiment of Ref. 35, and the histogram is calculated.

## ENERGY DEPOSITION IN THIN LAYERS OF Si AND GaAs

As an example of using this model to calculate radiation damage to semiconductor materials, let us consider the interaction of protons, $\alpha$ particles, and multiply charged ions with thin layers of silicon and gallium arsenide at $E=3.65$ GeV/nucleon. The measurements for silicon were carried out at the synchrophasotron of the JINR High Energy Laboratory.[42]

In Fig. 14 we show the construction of the target incorporating a surface-barrier detector with area of the sensitive volume 2.5 cm$^2$ and thickness 85 $\mu$m. The primary beam was made up of protons or $^{12}$C ions, or it was a mixture of $^4$He, $^7$Li, $^{10}$B, $^{12}$C, $^{14}$N, and $^{16}$O nuclei with relative content 18, 11, 1, 3, 6, 6, and 55%.

As already noted, the Monte Carlo method allows all the features of the experiment to be taken into account in detail.

The experimental and calculated spectra of the energy deposition in the sensitive layer of the detector bombarded by a proton beam

$$N(\Delta E)=\frac{dN/dE}{\int_{\Delta E>1\text{MeV}}(dN/dE)dE} \tag{8}$$

is shown in Fig. 15. In Fig. 16 we compare the energy losses in proton and ion beams.

The experimental spectra are approximated well by the sum of two exponentials:

$$N(\Delta E)=a_1\exp(-b_1\Delta E)+a_2\exp(-b_2\Delta E) \tag{9}$$

with the exponents $b_1$ and $b_2$ given in Table IV. The theoretical spectra have the same form. The calculated values agree with the experimental ones within the errors.

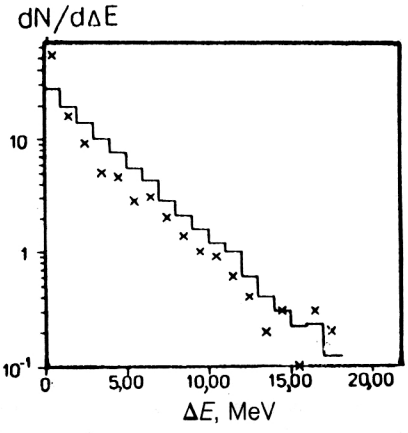


FIG. 10. Experimental distribution of residual nuclei in the reaction $p+^{28}Si$ for $E=100$ MeV. The histogram is the calculation of Ref. 39, and the $\times$ are our data.

We see from Table IV and Fig. 16 that the shape of the high-energy part of the spectrum for $\Delta E > 5$ MeV, which is most important from the viewpoint of radiation-induced damage to semiconductor devices, is determined by the contribution of the slowly falling exponential and depends very weakly on the type of bombarding particle. At the same time, energy depositions $\Delta E < 3$ MeV depend strongly on the type of particle. The average energy losses $\langle E \rangle = 1$ and 5 MeV, corresponding to the two exponentials over the sensitive length of the detector equal to 85 $\mu$m, are related to specific energy losses $dE/dx$ of order 0.1 and 1 GeV/$c$, respectively, which are characteristic for $\alpha$ particles and ions with charge number $Z=7$ and energy 10–20 MeV. The calculations show that the characteristics of multiply charged fragments and nuclei depend comparatively weakly on the type of primary particle, which leads to stability of the energy-loss tail.

We see from Fig. 15 that the relative values of the calculated energy-deposition spectra are in good agreement with the experimental ones. In addition, the absolute values $N(\Delta E)$ are somewhat smaller than the measured ones. Moreover, at small $\Delta E$ they are noticeably less sensitive to the type of bombarding particle (cf. Fig. 13 and Table IV). The reason for the disagreement is not yet clear.

Let us now consider the energy deposition in thin layers of gallium arsenide. The target geometry is as in Fig. 13, but GaAs is used instead of silicon.

In Fig. 17 we compare the calculated energy-deposition spectra for Si and GaAs bombarded by protons and $^{12}C$ ions. These and all the data given below pertain to the energy $E=3.65$ GeV/nucleon. We see that the replacement of silicon by gallium arsenide leads to an increase of the energy deposition. There are three main reasons for this: 1) the increase of the macroscopic cross section for the interaction of the bombarding particles with the target material, $\Sigma_{in}$, which in the case of thin targets is roughly the same for all $\Delta E$; 2) the more developed hadron–meson cascade formed in inelastic nuclear collisions, which is mainly related to small values of $\Delta E$; 3) the large contribution from heavy fragments in the case of GaAs bombarded by a proton beam, which does not break up the target nucleus as strongly as a heavy-ion beam.

The relative importance of these three factors is clearly

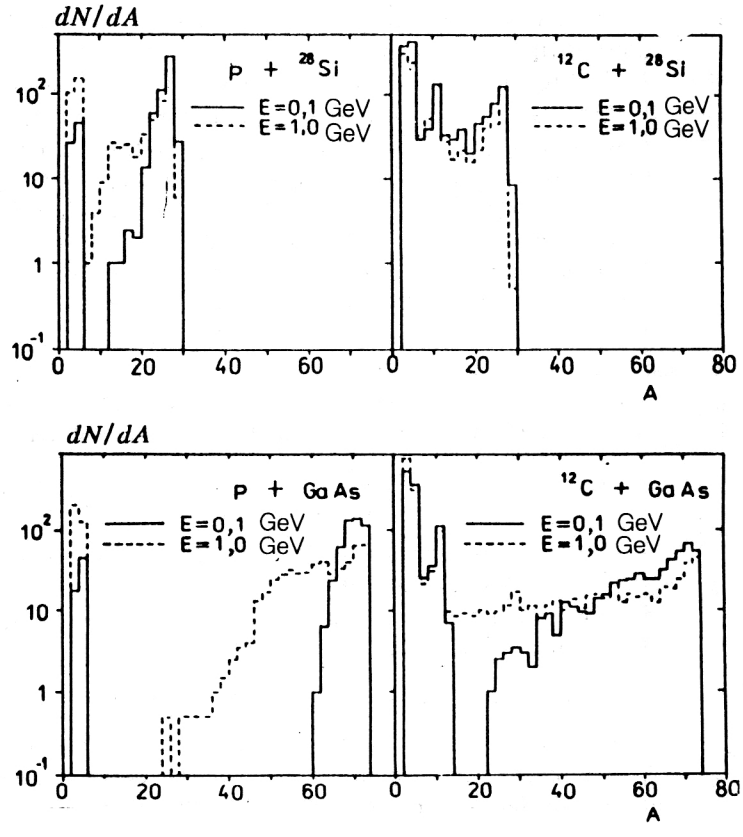


FIG. 11. Mass-number distribution of fragments and recoil nuclei. The solid- and dashed-line histograms are the calculation for the energy of the bombarding protons and $^{12}C$ ions equal to $E=0.1$ and 1 GeV/nucleon.

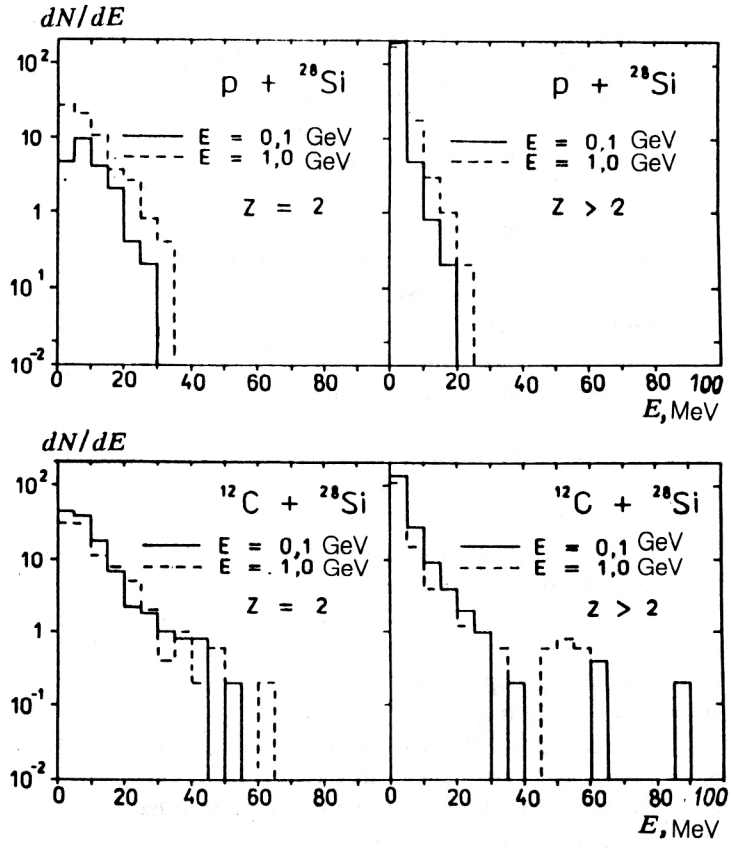


FIG. 12. Energy spectra of $\alpha$ particles ($Z=2$) and nuclei with $Z>2$ produced in interactions of protons and $^{12}C$ ions with $^{28}Si$ nuclei. The solid- and dashed-line histograms are the calculation for $E=0.1$ and 1 GeV/nucleon.

seen from Fig. 18, where we give the cross-section-independent frequency ratios:

$$W(\Delta E)=\frac{N(\Delta E)_{GaAs}}{N(\Delta E)_{Si}}\frac{\Sigma_{in}^{(Si)}}{\Sigma_{in}^{(GaAs)}}. \quad (10)$$

For $\Delta E=2$–6 MeV the ratios are close to unity, and at larger and smaller $\Delta E$, respectively, the other two factors contribute.

Although the energy release induced by $^{12}C$ ions is

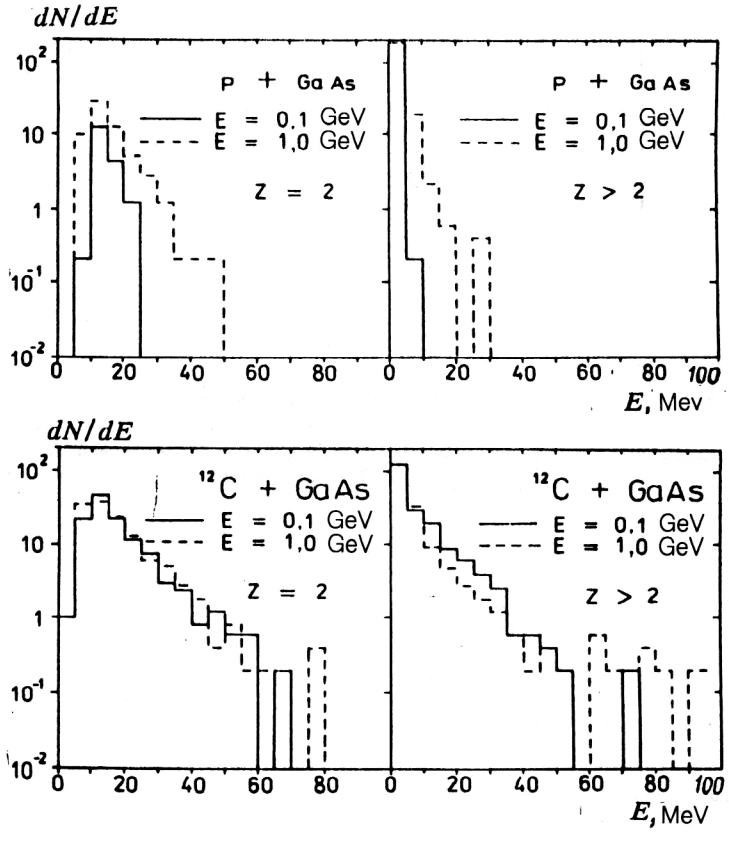


FIG. 13. The same as in Fig. 12. Interactions with GaAs nuclei.

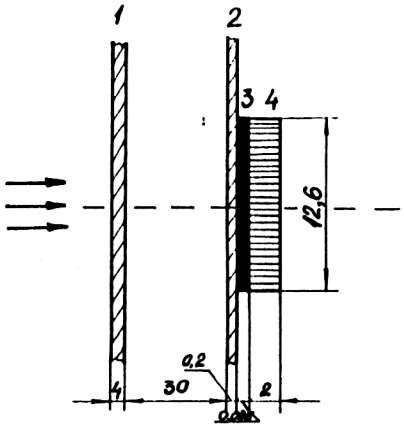


FIG. 14. Target geometry. *1*) Aluminum screen [the measurements were performed simultaneously with another experiment; the screen distorts the values of $N(\Delta E)$ only for $\Delta E < 2$ MeV]; *2*) a sheet of paper cutting off low-energy $\alpha$ particles; *3*) sensitive volume of the silicon detector; *4*) silicon backing. All dimensions are given in millimeters.

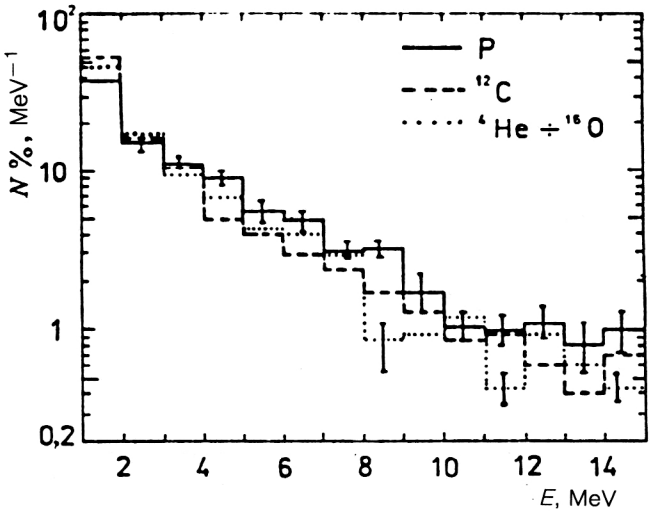


FIG. 16. Dependence of the energy-deposition spectrum on the type of bombarding particle. The statistical errors of the calculation are shown.

noticeably larger than in a proton beam, the uniformly normalized probabilities

$$N_0(\Delta E)=\frac{N(\Delta E)}{\Sigma_{\Delta E>2\text{MeV}}N(\Delta E_i)} \tag{11}$$

are practically independent of the type of bombarding particle (see Fig. 19).

Just as in the case of silicon, the full energy-deposition spectrum for GaAs is described by the sum of two exponentials. Here the exponent of the most important, slowly falling exponential can be assumed to be independent of the type of bombarding particle. This makes it possible to estimate the number of upsets in different types of beam.

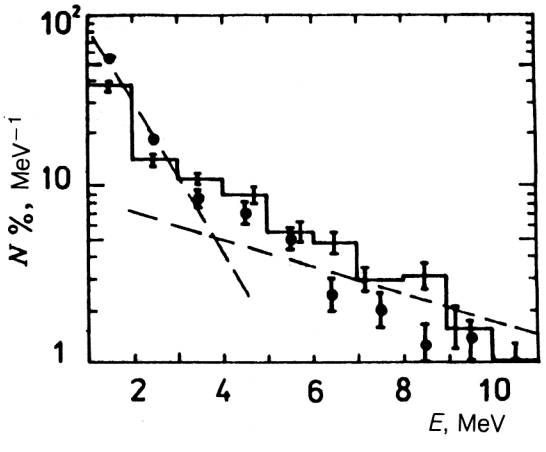


FIG. 15. Probability of depositing an energy $\Delta E$ in the sensitive layer of the detector.[42] The primary beam is a proton beam. The points are the measurement results, and the histograms are calculated. The dashed lines are the approximation (8) with parameters from Table IV. For absolute calibration of the experimental values it is necessary to take into account the fact that in the range $\Delta E=1$–2 MeV for one primary proton $N(\Delta E)=1.28\times10^{-3}$; $a_1=1.3$; $a_2=0.087$.

## THE MODELING OF LAYERS IN MICROCIRCUIT CELLS

Let us now consider a more complicated case: the probability of radiation-induced upsets in a silicon microcircuit consisting of 4000 cells of thickness 100 $\mu$m on a silicon backing. As in the cases considered earlier, we shall assume that the primary particles bombarded the target in the direction perpendicular to its surface.

In actual semiconductor circuits the volume sensitive to radiation damage, which depends on the construction of the device, is somewhat smaller than the geometrical volume of a cell. We shall not take this difference into account for now. As the threshold energy we use the value $\Delta E=2$ MeV (see Fig. 1).

In Fig. 20 we show the calculated distributions of the number of damaged cells in the value of the energy deposited in them $N(\Delta E)/N_{\text{tot}}$, where

$$N_{\text{tot}}=\int_{\Delta E>2\text{MeV}}(dN/dE)dE \tag{12}$$

is the total number of damaged cells. In Fig. 21 we show the corresponding integrated distributions

$$N(>\Delta E)=\int_{\varepsilon>\Delta E}N(\varepsilon)d\varepsilon/N_{\text{tot}}. \tag{13}$$

As in thin semiconductor layers, the energy deposited in a cell depends weakly on the type of bombarding particle. In roughly half the cases of proton bombardment and

TABLE IV. Coefficients of the exponential approximation for the experimental energy-deposition spectra.

| Particle | $b_1$ | $b_2$ |
|---|---|---|
| $p$ | $0.950\pm0.005$ | $0.160\pm0.01$ |
| $^{12}$C | $1.8^{+0.4}_{-0.3}$ | $0.20\pm0.01$ |
| $^4$He−$^{16}$O | ··· | $0.190\pm0.02$ |

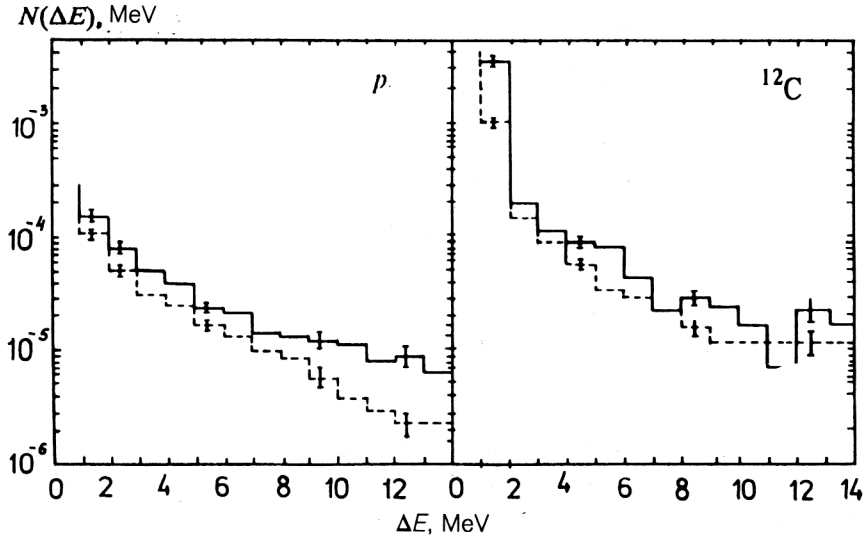


FIG. 17. Calculated number of cases of energy deposition $\Delta E$ per bombarding particle (a proton or a $^{12}C$ ion). The solid-line histograms are for GaAs, and the dashed-line ones are for Si.

about 60% of the cases of $^{12}C$ bombardment an energy $\Delta E = 2$–4 MeV is deposited in a cell. The probability for a very large energy deposition ($\Delta E > 10$ MeV) is only about 3–4% in the two cases.[6]

To understand the mechanism for radiation damage and to further improve the physical aspects of the model, it is important to know which particles—cascade hadrons, multiply charged fragments of decaying nuclei, or recoil nuclei—give the dominant contribution to the energy release. For this in Fig. 22 we show the relative contribution to the probability for radiation damage of a cell (i.e., for the deposition in it of an energy $\Delta E > 2$ MeV) by various types of charged particle produced in the internuclear cascade process.

The negligible (5–7%) contribution of singly charged particles—cascade protons, mesons, deuterium and tritium nuclei—should be noted. This contribution is small because most of these particles have high energy, so they very weakly ionize the medium. The main contribution (40–60%) comes from doubly charged helium ions, and heavy multiply charged recoil nuclei formed in nonequilibrium pre-compound decays and "evaporation" of post-cascade nuclei give a contribution nearly as large (Fig. 23). Since protons break up the target nucleus more weakly, the relative contribution of helium ions in this case is smaller, and the contribution of recoil nuclei with charges close to the initial value is larger than in bombardment by carbon ions.

In Figs. 24 and 25 for the example of a proton beam (similar results are obtained for ions) we compare the charge and energy distributions calculated with and without the preequilibrium decay of post-cascade nuclei. The differences in the charge distributions are unimportant. The ten-percent discrepancy in the $\alpha$-particle contribution arises from the fact that preequilibrium processes lower the excitation energy of the residual nuclei, which causes the probability for "evaporation" of $\alpha$ particles, which are heavier than nucleons, to decrease as well. The differences in the energy histograms are more noticeable. The nonequilibrium fragments emitted by nuclei, as a rule, have higher energy than evaporation particles and, on the average, generate a larger energy release in the cells. This indicates that the calculations of radiation damage must be carried out with inclusion of nonequilibrium processes.

It should also be borne in mind that the probability for radiation-induced upsets is very sensitive to the dimensions and geometry of the microcircuit. For example, for the microcircuit that we considered with transverse dimensions $0.2 \times 0.5$ cm and thickness $d = 100$ $\mu$m, singly

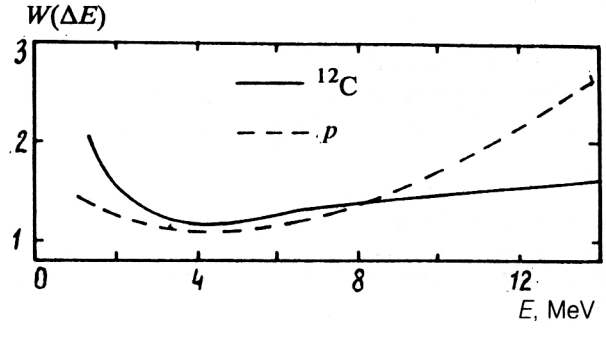


FIG. 18. Cross-section-independent ratios of energy deposition frequencies in gallium arsenide and silicon. The solid line is the calculation for a beam of carbon ions, and the dashed line is for a proton beam.

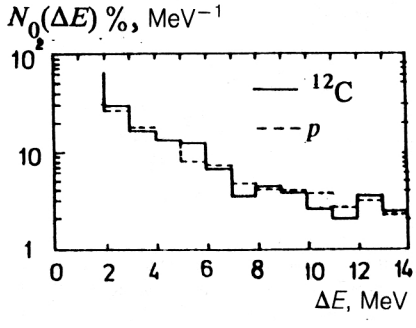


FIG. 19. Uniformly normalized probabilities for energy deposition in a layer due to a beam of $^{12}C$ ions (solid-line histogram) and a proton beam (dashed-line histogram).

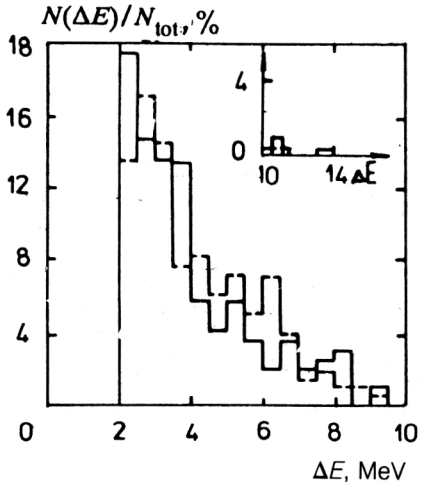


FIG. 20. Relative number of microcircuit cells in which protons (dashed-line histogram) and $^{12}C$ ions (solid-line histogram) have deposited an energy $\Delta E$. The statistical reliability of the calculations is 1000 primary proton interactions in the cell layer and the 299 $\mu$m silicon backing, as a result of which 198 cases of cell damage occurred; correspondingly, there were 190 cases of cell damage for 1113 $^{12}C$ ions.

charged particles produce upsets only for $\Delta E < 3$ MeV, while for a circuit of dimensions $1 \times 1.25$ cm and $d = 85$ $\mu$m their contribution in the region $\Delta E < 3$ MeV is about 60%. The distribution of upsets induced by a large energy deposition is changed insignificantly. In other words, each case requires mathematical modeling.

## MODELING OF RADIATION-INDUCED DAMAGE TO MICROSTRIP DETECTORS

As yet another application of the model that we have developed, let us consider the calculation of radiation defects (atoms knocked out of crystal lattices) in a silicon

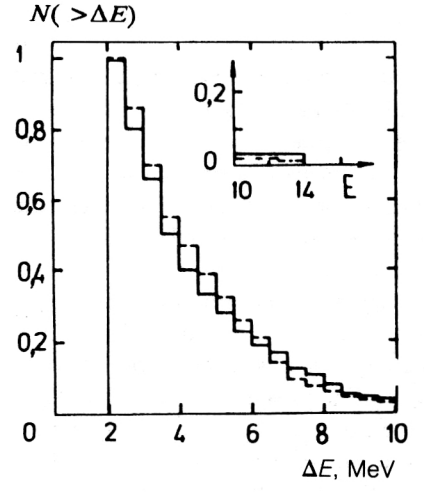


FIG. 21. Relative number of microcircuit cells with energy deposition greater than $\Delta E$. The solid-line histogram is for a $^{12}C$ ion beam, and the dashed-line one is for a proton beam. The statistical reliability is the same as in Fig. 20.

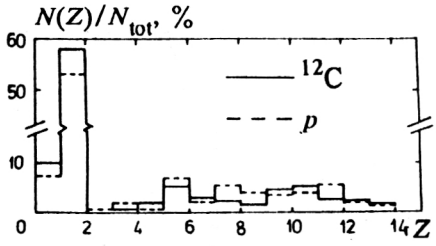


FIG. 22. Probability of depositing in a cell a radiation energy $E > 2$ MeV by a cascade particle of charge $Z$.

microstrip detector bombarded by high-energy carbon ions ($E = 3.65$ GeV/nucleon) and a neutron beam with energy $E = 10.5$ MeV.

The number of knocked-out atoms depends on the type and energy of bombarding particle, and so, in general, various experiments are necessary to measure it. However, if the relations between defect-production in different beams are known, the expected efficiency can be estimated under simpler conditions, for example, by bombarding the detector with an intense beam of reactor neutrons.

In order to see whether such conversion is possible, let us consider a silicon film of thickness 3000 $\mu$m bombarded by a needle-shaped beam of particles at perpendicular incidence with a given energy $E$. We use the 26-group system of neutron constants[12] and data on the $(n,p)$ and $(n,\alpha)$ reactions. We shall assume that $\alpha$-particle production occurs only within the first group ($E = 10.5$–$6.5$ MeV) with a cross section of 91 mb (Ref. 48). The $(n,p)$ cross sections are given in Table V. Owing to the absence of reliable experimental data, we assume that the energy distributions of protons and $\alpha$ particles are the same as for neutrons in inelastic reactions: the energies are distributed according to the cross sections for inelastic transitions from one group to another, and within a single group the energy will be selected randomly with equal probability. We shall assume that the proton and $\alpha$-particle angular distributions are

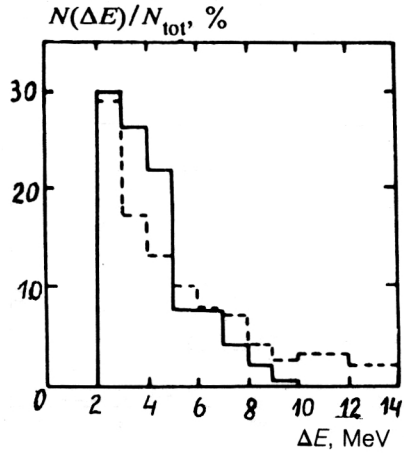


FIG. 23. Probability of radiation-energy deposition in a cell by $\alpha$ particles (solid-line histogram) and nuclei with charge $Z > 2$ (dashed-line histogram).

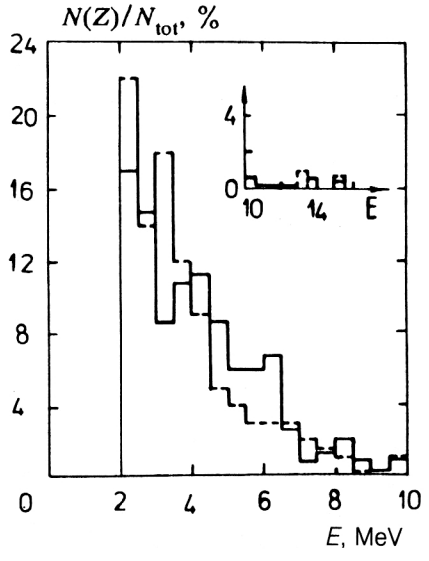


FIG. 24. Energy deposition in a microcircuit cell bombarded by protons of energy $E=1$ GeV. The solid-line histogram was calculated using the evaporation model augmented by nonequilibrium decays, and the dashed line is the calculation neglecting these decays.

isotropic. The momentum vector of the recoil nucleus is determined by energy–momentum conservation.

To economize on computer time, we use the statistical weight (2), as in the preceding sections.

The number of atoms knocked out of the lattice by a multiply charged ion with kinetic energy $E$ is

$$N(E)_{\text{def}}=\frac{1}{2E_d}\int_0^E \frac{(dE/dx)_{\text{el}}}{(dE/dx)_{\text{tot}}dE}, \tag{14}$$

where $E_d=13$ MeV is the threshold energy of the atomic displacement and $dE/dx$ is the energy lost in electromagnetic processes.[49,50] At energies above some value $T_1$ depending on the charge and mass of the initial ion, the charge screening of the nucleus is unimportant, and the elastic losses are determined by the Rutherford-scattering cross section and the weakly (logarithmically) energy-dependent primary-defect multiplication coefficient.[51] At lower energies in the calculation of losses due to elastic

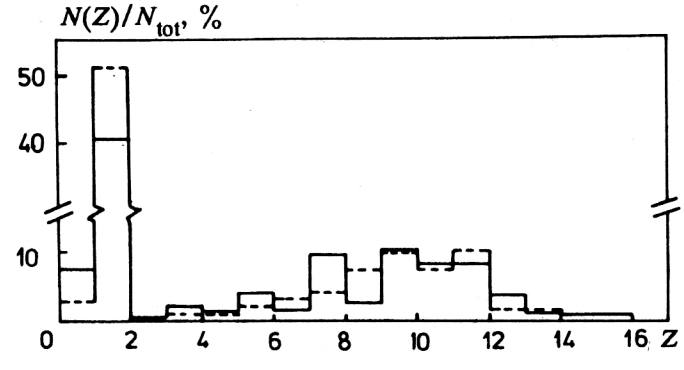


FIG. 25. Probability for the deposition in a microcircuit cell of an energy $\Delta E>2$ MeV by a particle of charge $Z$. The primary beam is a proton beam with $E=1$ GeV. The notation is the same as in Fig. 24.

TABLE V. Cross sections for proton production by a neutron of energy $E$.

| Group number | 1 | 2 | 3 | 4 | 5 |
|---|---|---|---|---|---|
| $E$, MeV | 10.5–6.5 | 6.5–4 | 4–2.5 | 2.5–1.4 | 1.4 |
| $\sigma$, mb | 123 | 236 | 162 | 71 | 0 |

scattering of the atoms it is necessary to take into account atomic-screening effects. In this region we have used for $dE/dx$ the analytic approximation[18] of the results obtained using the Thomas–Fermi theory in Ref. 13. For protons and $\alpha$ particles the values of $T_1$ were obtained in Ref. 51, and for the other ions we used the expression

$$T_1=0.01Z^{2/3}, \tag{15}$$

where $Z$ is the charge of the incident ion.

In Fig. 26 we show the calculated energy dependences of the mean free path of the bombarding particles, the total number of defects produced by a particle of energy $E$ before it completely stops in the detector material or leaves the detector, and the corresponding production density at energy $E$ calculated for 1 cm. In the case of protons and $\alpha$ particles these dependences are close to those given in Ref. 51. The data for $^{28}$Si ions are characterized by defect production due to recoil nuclei, which give a very important contribution to the total defect production. We see that the replacement of a proton by an $\alpha$ particle increases the number of defects by about an order of magnitude, and the use of silicon ions increases their number by another factor of five.

In Fig. 27 we show the spatial distribution of the defects $\Delta N/\Delta S$, where $\Delta S=\pi(r_2^2-r_1^2)-2\pi r\Delta r$, $r$ being the distance from the axis of the primary particle beam at perpendicular incidence. There we also give the following approximating curves calculated by the rms method:

$$\Delta N/\Delta S=ar^b,$$

where $a=8.14\times10^7$ and $b=2.82$ for protons and $a=5.76\times10^9$ and $b=3.88$ for neutrons.

The number of defects formed in a neutron beam exceeds the number of defects formed by protons at $E=3.65$ GeV by almost two orders of magnitude. However, the spatial distributions in these cases do no differ very significantly.

In Fig. 27 we show separately the contributions of particles with electric charges $Z=1$, $Z=2$, and $Z>2$. In a neutron beam the recoil nuclei give a contribution only near the axis $Z\cong0$, while in proton bombardment their contribution is noticeable up to a fraction of a millimeter.

Comparison of the calculated values like those shown in Fig. 27 makes it possible to arrive at some conclusion about the possibility of mimicking the efficiency of strip detectors by replacing some beams by others which are more convenient for experimental studies.[6]

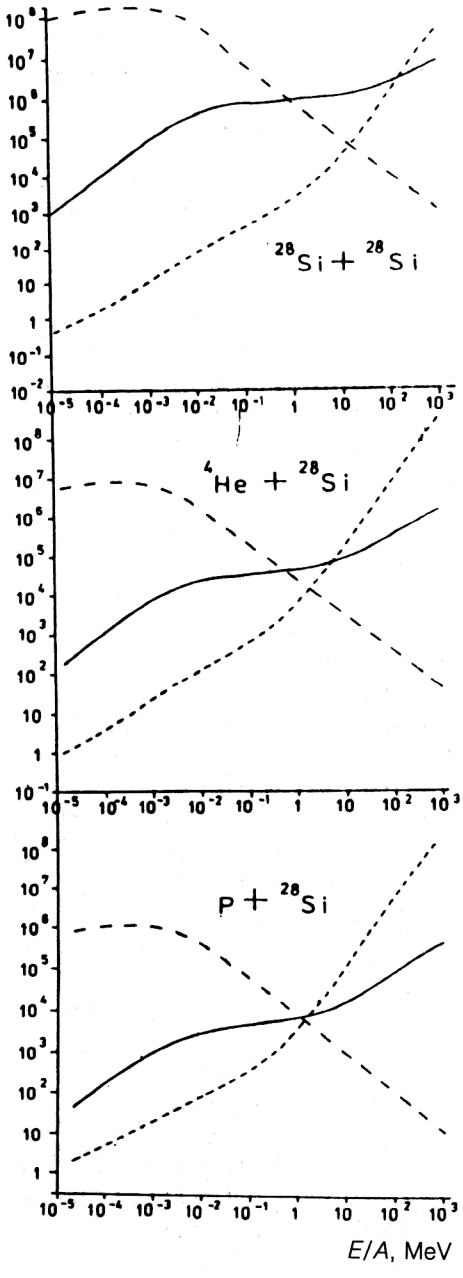


FIG. 26. Mean free path of the bombarding particle $R$ (in cm), defect-formation density $n_{def}$ (in 1/cm), and total number of defects produced $N_{def}$; $E$ is the energy of the bombarding particle. The solid line is the number of defects ($\times 10^2$), the line with small dashes is the mean free path (in cm), and the line with large dashes is the defect density (in 1/cm).

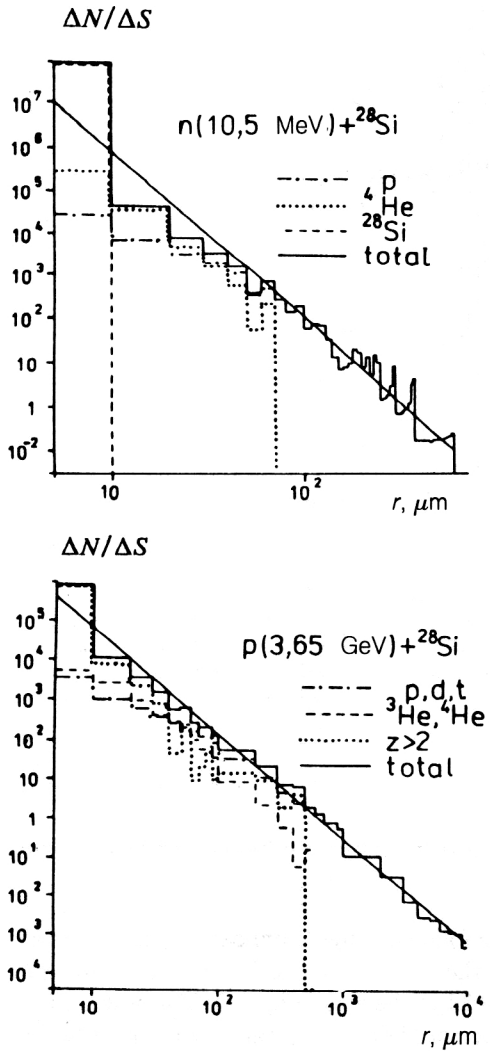


FIG. 27. Radial distribution of defects. The distributions resulting from various types of cascade particles are shown.

## RADIATION-INDUCED DAMAGE TO HTSC BOLOMETERS

The technology of high-temperature superconducting (HTSC) thin-film materials makes it possible to convert highly sensitive and fast electromagnetic radiation devices from liquid-helium to liquid-nitrogen temperatures, which reveals new possible applications of them, in particular, in fields of strongly ionizing cosmic rays and artificial radiation.[52–56] However, here the following questions arise: first, does the heat release in different parts of HTSC devices generated by secondary-particle showers tend to worsen their operating parameters and, second, how do these devices behave at very large radiation doses?

As a particular example of the mathematical modeling of the action of high-energy ions on HTSC bolometers, the authors of Refs. 46 and 47 considered a bolometer with a sensitive HTSC element made of $YBa_2Cu_3O_{7-x}$ on a backing of strontium titanate $SrTiO_3$. In Figs. 28 and 29 we show the construction of such a bolometer with a nitrogen cryostat and its intake, and in Fig. 30 we show the geometry for modeling them used in our calculations of radiation-induced heat deposition. It takes into account all the construction elements and the device dimensions, except for several inessential simplifications (replacement of rectangular parts by cylindrical ones, neglect of the film contacts, and so on).

Like the cases considered above for microelectronic devices, a special feature of the geometry in Fig. 30 is the presence of components with thickness less than the average nuclear mean free path of the particles, and therefore to ensure that the calculations are sufficiently accurate it is again necessary to use specially chosen statistical weights.

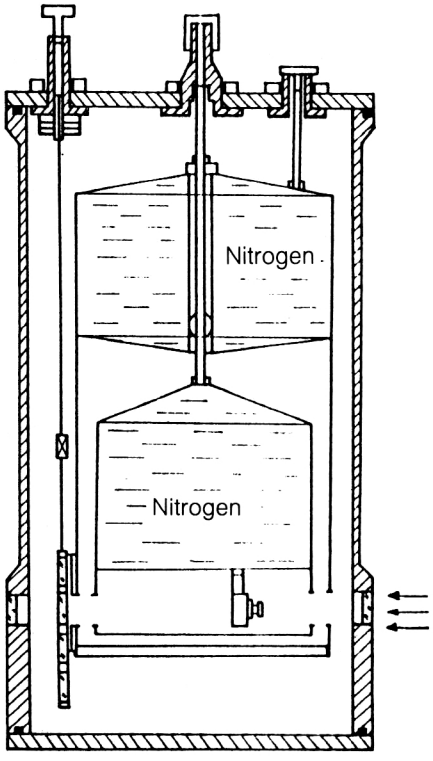


FIG. 28. Schematic diagram of a bolometer based on an ÉV-214 cryostat.

For example, the following algorithm can be used. First we assume that all the particles move in the same direction along a line parallel to the axis (Fig. 30). For now we also neglect the change of their energy (and, consequently, the interaction probability) due to ionization processes in the intervals between nuclear collisions. Then the collision probability for a particle inside the $i$th part of the apparatus in question is

$$\omega_i=\xi_{i-1}-\xi_i, \quad \xi_i=\exp\left(-\sum \Delta l_j(\lambda_j)\right),$$

where $l_i$ and $l_{i-1}$ are the coordinates of the end and the beginning of this part ($l=0$ is the coordinate of the entrance point, and $\Delta l_i=l_i-l_{i-1}$ is the thickness of the $i$th part), and $\lambda_i$ is the mean free path in the material of a given part. The actual number of the part in which the particle interacted is randomly selected, using a random-

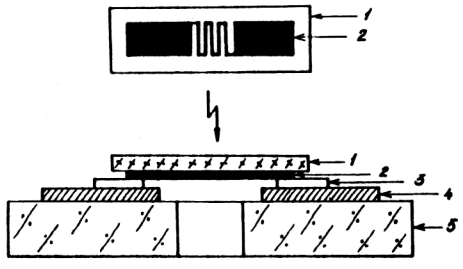


FIG. 29. Construction of an intake for a HTSC bolometer. *1*) Backing; *2*) HTSC film; *3*) contactor; *4*) polycore; *5*) glass.

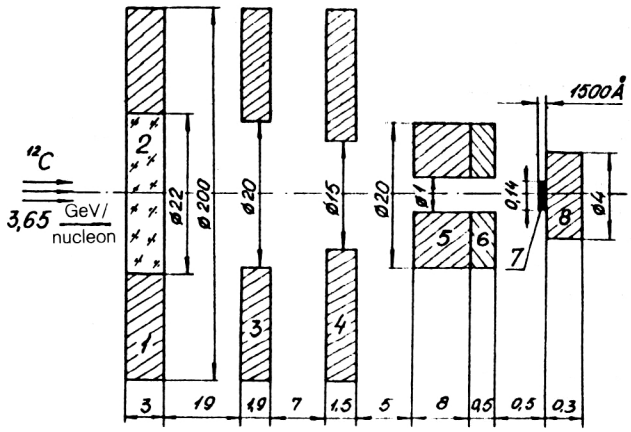


FIG. 30. Geometry used in the mathematical modeling of radiation energy deposition in parts of the bolometer. The dimensions are given in millimeters, and the thickness of the HTSC film is given in angstroms. The chemical composition and numbering of the parts are given in Table VI.

number generator for numbers randomly distributed in the interval [0,1]. Here for thin parts, for which $\Delta l_i/\lambda_i \ll 1$, $\omega_2=1$. This is precisely the difficulty which arises in direct modeling. To avoid it, we introduce the formal (weighting) probabilities $\omega_{pi}$; for example, we assign equal probabilities to all parts of the device: $\omega_{pi}=1/8$. We use these probabilities to randomly select the numbers of the parts in which cascade particles interact and the coordinates of the interaction points:

$$l=l_{i-1}-\lambda \ln[\xi_i+\gamma(\xi_{i-1}-\xi_i)],$$

where $\gamma$ is a uniformly distributed random number chosen anew each time.

The true values of the desired quantities (in this case the heat deposited in each of the eight parts) are found by multiplying the values calculated using the probabilities $\omega_{pi}$ by the statistical weights $p_i=\omega_i/\omega_{pi}$, i.e., $X_i=X_{pi}p_i$.

The generalization of the algorithm to the case of three-dimensional geometry is trivial. The change of the mean free paths due to ionization losses can be taken into account using the above-mentioned cross-section equalization method, by additional rejection of fictitious interactions. This method allows the simple inclusion of the presence of empty ($\lambda=0$) regions between parts of the device.

Since in the experiment of Refs. 46 and 47 a broad ion beam was used which covered not only the entrance window of the cryostat, but also a significant part of its adjacent walls, a statistical weight (equal to the ratio of the window area and the included part of the wall with radius 10 cm) was introduced to take into account the contribution of the ions which enter the cryostat through the relatively weakly absorbing quartz glass. In Table VI we give the calculated heat depositions in all the parts of the device shown in Fig. 30.

We see from this table that the main heat deposition occurs in the walls of the cryostat and in the aluminum screens. However, only the heat deposited in the actual head of the bolometer (parts 5–8 in Fig. 30) is important

TABLE VI. Heat deposition in parts of the cryostat and bolometer calculated for $10^3$ $^{12}C$ nuclei [in $(cm^2 \cdot s)^{-1}$].

| Construction part | Material | $E$, MeV |
|---|---|---|
| Cryostat wall | Al | $2.6\times10^{-4}$ |
| Entrance window | $SiO_2$ | 93 |
| Screen | Al | $1.6\times10^{-4}$ |
| Screen | Al | $1.5\times10^{-4}$ |
| Bolometer container | Cu | $7.7\times10^{-2}$ |
| Bolometer base | $Al_2O_3$ | 15 |
| Sensitive element | $YBa_2Cu_3O_{7-x}$ | $9.4\times10^{-6}$ |
| Backing | $SrTiO_3$ | $6.3\times10^{-4}$ |

for the operation of the device. Knowing the total amount of heat deposited in this part of the device, $Q=S\Sigma Q_i$ ($S$ is the area of the ion beam, and the coefficient of heat loss from the bolometer container to the bottom of the cryostat is $G$; in our case $G=2\times10^{-2}$ W·K$^{-1}$), it is possible to find the excess heating of the bolometer relative to the bottom of the cryostat: $\Delta T=Q/G=5\times10^{-6}$ [calculated for the ion flux used in the experiment of Refs. 44, 45, and 56: 800 ions $(cm^2 \cdot s)$]. It makes up an insignificant fraction of the transition width $\Delta T_c \cong 1.2$ K. It follows from comparison with the experimental characteristics of the bolometer that such temperature variations cannot noticeably affect the bolometer sensitivity. Variations of the working temperature $\Delta T \geqslant 0.1$ K (a 10% change of sensitivity) are needed for this, and accordingly, the intensity of the $^{12}C$ ion beam is roughly $10^7$–$10^8$ ions/$cm^2 \cdot s$). The critical intensity is lower for heavier ions.

The calculation shows that the radiation heating of the bolometer has an important dependence on its construction details. For example, an increase of the container and base dimensions of the bolometer ($i=5,6$) to 10 cm raises the temperature $\Delta T$ by two orders of magnitude, to $6\times10^{-4}$ K. Replacement of the aluminum screens ($i=3,4$) by copper ones increases $\Delta T$ by 10–15%.

## CONCLUSIONS

It follows from the data given above that the cascade model that we have developed allows the study of various aspects of radiation damage of semiconductor microelements by particles of widely varying energy—up to very high energies of the order of several tens of GeV/nucleon.

The more correct inclusion of quark–gluon processes makes it possible to extend the model to even higher energies. However, the most important future improvements will primarily be related to improvement of the theory of the decay of the excited (residual) nuclei produced in the cascade process and the inclusion of the curvature and the statistical spread of the lengths of the tracks of low-energy particles at short distances of the order of several micrometers and below.

More reliable testing of the model will require further experiments to measure the number of radiation-induced upsets at various values of the threshold energy and for various energies and types of bombarding particle.

In conclusion, we consider it our pleasant duty to thank L. N. Zaĭtsev for advice and stimulating criticism.

[1)] At high incident particle energies, the average energy of $\alpha$ particles produced in the internuclear cascade process (including those from the "evaporation" of post-cascade excited recoil nuclei) is about 10 MeV, which corresponds to a mean free path in silicon of 70–80 $\mu$m. The mean free paths of heavier nuclear components of the cascade are considerably smaller (about 1–10 $\mu$m). Therefore, only the first 200–300 $\mu$m of the backing are important. Accordingly, the curve $N(d)/N(0)$ flattens out to a plateau for $d \cong 300$ $\mu$m.

[1] D. Binder, E. C. Smith, and A. B. Holman, IEEE Trans. Nucl. Sci. **NS-22**, 2675 (1975).
[2] V. I. Astakhov, A. Bishoff, A. S. Vodop'yanov *et al.*, Report R13-90-7, JINR, Dubna (1990) [in Russian].
[3] D. V. Akin'shin, M. N. Borisova, N. G. Goleminov *et al.*, Prib. Tekh. Eksp. No. 6, 49 (1990) [Instrum. Exp. Tech.].
[4] N. G. Goleminov, V. I. Ivanov, and E. A. Kramer-Ageev, At. Energ. **49**, 373 (1980).
[5] N. G. Goleminov and E. A. Kramer-Ageev, *Problems in Microdosimetry* [in Russian] (Énergoatomizdat, Moscow, 1982), p. 68.
[6] V. S. Barashenkov *et al.*, Zh. Tekh. Fiz. **60**, No. 10, 75 (1990) [Sov. Phys. Tech. Phys. **35**, 1158 (1990)].
[7] V. S. Barashenkov, Report R2-81-364, JINR, Dubna (1981) [in Russian].
[8] V. S. Barashenkov, Lee Van Ngoc, L. G. Levchuk *et al.*, Report R2-86-226, JINR, Dubna (1986) [in Russian].
[9] V. S. Barashenkov, Report R2-90-148, JINR, Dubna (1990) [in Russian]; Report R2-90-158, JINR, Dubna (1990) [in Russian].
[10] V. S. Barashenkov, A. Polanski, and A. N. Sosnin, Report R2-89-753, JINR, Dubna (1989) [in Russian]; Report R2-90-159, JINR, Dubna (1990) [in Russian].
[11] V. S. Barashenkov, Report R2-90-257, JINR, Dubna (1990) [in Russian].
[12] L. P. Abagyan, N. O. Bazazyants, M. N. Nikolaev *et al.*, *Group Constants for Reactor and Shielding Calculations* [in Russian] (Énergoatomizdat, Moscow, 1981).
[13] L. Lindhard, M. Scharff, and H. E. Schiott, K. Dan. Vidensk. Selsk. Mat.-Fys. Medd. **33**, No. 14 (1963).
[14] S. V. Starodubtsev and A. M. Romanov, *Passage of Charged Particles Through Matter* [in Russian] (Uzbek Academy of Sciences, Tashkent, 1962).
[15] R. Sternheimer, Phys. Rev. **145**, 247 (1966); B **3**, 3681 (1971).
[16] M. Walske, Phys. Rev. **88**, 1283 (1952); **101**, 940 (1956).
[17] D. C. Santry and R. D. Werner, Nucl. Instrum. Methods B **1**, 13 (1984); **15**, 47 (1986).
[18] V. S. Barashenkov, A. Polyanski, A. N. Sosnin, and S. Yu. Shamkov, Dep. Publ. B1-2-91-93, JINR, Dubna (1991) [in Russian].
[19] E. L. Potemkin, V. V. Smirnov, and V. V. Frolov, Yad. Fiz. **27**, 900 (1978) [Sov. J. Nucl. Phys. **27**, 478 (1978)].
[20] B. I. Goryachev and N. V. Lin'kova, Yad. Fiz. **49**, 1046 (1989) [Sov. J. Nucl. Phys. **49**, 647 (1989)].
[21] A. Van Ginneken, Nucl. Instrum. Methods A **251**, 21 (1986).
[22] C. C. Northcliffe and R. F. Schilling, Nucl. Data Tables A **7**, 233 (1970).
[23] F. Hubert, R. Bimbot, and H. Gauvin, At. Data Nucl. Data Tables **46**, 1 (1990).
[24] S. M. Ermakov and G. A. Mikhaĭlov, *Statistical Modeling* [in Russian] (Nauka, Moscow, 1982).
[25] V. S. Barashenkov and V. D. Toneev, *Interactions of High Energy Particles and Nuclei with Nuclei* [in Russian] (Atomizdat, Moscow, 1972).
[26] V. S. Barashenkov, A. S. Il'inov, N. M. Sobolevskiĭ, and V. D. Toneev, Usp. Fiz. Nauk **109**, 91 (1973) [Sov. Phys. Usp. **16**, 31 (1974)].
[27] V. S. Barashenkov, B. F. Kostenko, and A. M. Sadorozhny, Nucl. Phys. **A338**, 413 (1980).
[28] V. S. Barashenkov, F. G. Zheregi, and Zh. Zh. Musul'manbekov, Yad. Fiz. **39**, 1133 (1984) [Sov. J. Nucl. Phys. **39**, 715 (1984)].
[29] E. Hermann *et al.*, Isotopenpraxis **6**, 259 (1990).
[30] X. Campi and J. Debois, in *Proc. of the Seventh High Energy Heavy Ion Study*, GSI Report, Darmstadt, 1985, p. 707.
[31] W. Bauer *et al.*, in *Proc. of the Seventh High Energy Heavy Ion Study*, GSI Report, Darmstadt, 1985, p. 701.

[32] V. V. Uzhinskii and S. Yu. Shmakov, Communication E2-89-581, JINR, Dubna (1989).
[33] A. Polanski, S. Yu. Shmakov, and V. V. Uzhinskii, Communication E2-88-793, JINR, Dubna (1988).
[34] S. Yu. Shmakov and V. V. Uzhinskii, Communication E2-87-780, JINR, Dubna (1987); S. Yu. Shmakov, N. V. Slavin, and V. V. Uzhinskii, Communication E2-88-792, JINR, Dubna (1988).
[35] V. S. Barashenkov, A. Polanski, and A. N. Sosnin, Communication E2-89-437, JINR, Dubna (1989).
[36] G. N. Agakishiev and D. Armutlijsky, Communication E1-84-321, JINR, Dubna (1984).
[37] T. Baatar, A. P. Gasparyan, V. G. Grishin *et al.*, Yad. Fiz. **36**, 431 (1982) [Sov. J. Nucl. Phys. **36**, 251 (1982)].
[38] D. Armutliiski, E. Bogdanovich, A. P. Gasparyan *et al.*, Report R1-86-263, JINR, Dubna (1986) [in Russian]; Report R1-87-905, JINR, Dubna (1987) [in Russian].
[39] J. Mougey, Nucl. Phys. **A387**, 109 (1982).
[40] V. S. Barashenkov, A. Polanski, A. N. Sosnin, and S. Yu. Shmakov, Communication E2-91-137, JINR, Dubna (1991).
[41] G. E. Farell, P. J. McNulty, and W. Abdel-Kader, IEEE Trans. Nucl. Sci. **NS-31**, 1073 (1984).
[42] V. S. Barashenkov, N. G. Goleminov, L. N. Zaitsev *et al.*, Nucl. Instrum. Methods B **58**, 157 (1991).
[43] V. S. Barashenkov, V. M. Pankov, A. N. Sosnin *et al.*, Communication E2-90-258, JINR, Dubna (1990); V. S. Barashenkov, A. V. Volchansky, L. N. Kondratev *et al.*, Communication E2-89-233, JINR, Dubna (1989).
[44] V. S. Barashenkov, A. N. Sosnin, P. I. Taranenko, S. N. Fedotov *et al.*, Reports R2-91-241, R2-91-242, JINR, Dubna (1991) [in Russian].
[45] V. S. Barashenkov, A. N. Sosnin, and S. Yu. Shmakov, Report R2-91-505, JINR, Dubna (1991) [in Russian].
[46] A. A. Astapov, V. S. Barashenkov, L. N. Zaĭtsev *et al.*, Report R7-90-241, JINR, Dubna (1990) [in Russian].
[47] V. S. Barashenkov, A. Polanski, A. N. Sosnin, and S. Yu. Shmakov, Report R7-91-29, JINR, Dubna (1991) [in Russian].
[48] V. G. Shchebolev and Z. A. Ramendik, At. Energ. **43**, 54 (1977).
[49] G. J. Dienes and G. H. Vineyard, *Radiation Effects in Solids* (Interscience, New York, 1957) [Russian transl., IL, Moscow, 1960].
[50] V. F. Kosmach *et al.*, Fiz. Tekh. Poluprovodn. **6**, 420 (1972) [Sov. Phys. Semicond. **6**, 364 (1972)].
[51] Yu. V. Bulgakov and M. A. Kumakhov, Fiz. Tekh. Poluprovodn. **2**, 1603 (1968) [Sov. Phys. Semicond. **2**, 1334 (1968)].
[52] I. A. Khrebtov, Prib. Tekh. Eksp. No. 4, 5 (1984) [Instrum. Exp. Tech.].
[53] M. G. Forrester *et al.*, Appl. Phys. Lett. **53**, 1332 (1988).
[54] S. V. Gaponov *et al.*, Pis'ma Zh. Tekh. Fiz. **14**, 1836 (1989) [Sov. Tech. Phys. Lett. **14**, 797 (1989)].
[55] S. V. Gaponov *et al.*, Pis'ma Zh. Tekh. Fiz. **15**, No. 12, 62 (1989) [Sov. Tech. Phys. Lett. **15**, 937 (1989)].
[56] A. A. Astapov *et al.*, Superconductivity **4**, 2043 (1991).

Translated by Patricia A. Millard